20. Schaible, H.-G. & Schmidt, R. F. *J. Physiol. (Lond.)* **403,** 91–104 (1988).
21. Graham, J. R. & Wolff, H. G. *Arch. Neurol. Psychiatr.* **39,** 737–763 (1938).
22. Friberg, L., Olesen, J., Iversen, H. K. & Sperling, B. *Lancet* **338,** 13–17 (1991).
23. Iversen, H. K., Nielsen, T. H., Olesen, J. & Tfelt-Hansen, P. *Lancet* **336,** 837–839 (1991).
24. Thomsen, L. L., Iversen, H. K. & Olesen, J. *Cephalalgia* **15,** 109–116 (1995).
25. Woolf, C. J. *Nature* **308,** 686–688 (1983).
26. Burstein, R., Malick, A. & Strassman, A. *Soc. Neurosci. Abstr.* **22,** 864 (1996).
27. Daley, M. L., Pasupathy, H., Griffith, M., Robertson, J. T. & Leffler, C. W. *IEEE Trans. Biomed. Eng.* **42,** 420–424 (1995).
28. Lauritzen, M. *Brain* **117,** 199–210 (1994).
29. Goadsby, P. J. & Edvinsson, L. *Ann. Neurol.* **33,** 48–56 (1993).
30. Orr, E. L. & Stokely, M. E. *Soc. Neurosci. Abstr.* **21,** 1858 (1995).

CORRESPONDENCE and requests for materials should be addressed to A.M.S. (e-mail: andrew strassman@bih.harvard.edu).

From stimulus encoding to feature extraction in weakly electric fish

F. Gabbiani*, W. Metzner†, R. Wessel‡ & C. Koch*

* Computation and Neural Systems Program, 139-74 Division of Biology, California Institute of Technology, Pasadena, California 91125, USA
† Department of Biology, University of California at Riverside, Riverside, California 92521, USA
‡ Department of Biology, University of California at San Diego, La Jolla, California 92093, USA

ANIMALS acquire information about sensory stimuli around them and encode it using an analogue or a pulse-based code. Behaviourally relevant features need to be extracted from this representation for further processing. In the electrosensory system of weakly electric fish, single P-type electroreceptor afferents accurately encode the time course of random modulations in electric-field amplitude[1]. We applied a stimulus estimation method[2] and a signal-detection method to both P-receptor afferents and their targets, the pyramidal cells in the electrosensory lateral-line lobe. We found that although pyramidal cells do not accurately convey detailed information about the time course of the stimulus, they reliably encode up- and downstrokes of random modulations in electric-field amplitude. The presence of such temporal features is best signalled by short bursts of spikes, probably caused by dendritic processing, rather than by isolated spikes. Furthermore, pyramidal cells outperform P-receptor afferents in signalling the presence of temporal features in the stimulus waveform. We conclude that the sensory neurons are specialized to acquire information accurately with little processing, whereas the following stage extracts behaviourally relevant features, thus performing a nonlinear pattern-recognition task.

The electric fish *Eigenmannia* generates a quasi-sinusoidal electric field with carrier frequencies between 200 and 600 Hz, by regularly discharging an electric organ located in its tail. The fish senses local distortions of the electric field by means of two classes of tuberous electroreceptors distributed on the body surface[3]: T-type and P-type electroreceptors encode changes in phase and electric field amplitude, respectively, which are used for electrolocation[4] and communication[5].

At the level of the electrosensory lateral line-lobe (ELL), the first central nucleus of the electrosensory pathway, amplitude information is processed nearly independently of phase information, and is re-encoded in the output spike trains of E- and I-type pyramidal cells[4,6]. The temporal response of P-receptor afferents and pyramidal cells has been characterized by their average firing rate for step changes and sinusoidal amplitude modulations of an externally applied electric field[4,7]. Under these conditions, the response of P-receptor afferents is slowly adapting (tonic), whereas the response of pyramidal cells is transient (phasic). Furthermore, P-receptor afferents and E-type pyramidal cells raise their mean firing rate when the electric field amplitude is increased, whereas I-type pyramidal cells are inhibited. These mean response characteristics leave open several alternatives for the encoding and processing of time-varying modulations in electric-field amplitude in single-spike trains of ELL pyramidal cells. Pyramidal cells might, for instance, transmit detailed information about the time course of temporal changes in the stimulus waveform[8], or of specific stimulus frequencies[9], combined with half-wave rectification.

To address the question of how modulations in electric-field amplitude are temporally encoded and processed between the first two stages of the amplitude pathway, we studied the responses of P-receptor afferents and pyramidal cells to random distortions of a mimic of the fish's own electric field. Such distortions were simulated by superposing zero-mean, random amplitude modulations, $s(t)$, to an externally applied electric field in fish whose electric-organ discharges were strongly attenuated by intramuscular injection of a curare-like drug (Fig. 1*a*). The carrier frequency of this field was equal to the fish's own frequency before the drug was applied, and the cut-off frequency of the random amplitude modulations[1] (Fig. 1*c*) was varied over a behaviourally relevant range (2–40 Hz) (refs 4, 10).

We assessed the ability of single-spike trains to convey detailed information about the time course of $s(t)$ by smoothing the time series of action potential events with a filter chosen to obtain the best estimate of $s(t)$ (refs 1, 2, 11). This method and its variants are able to detect detailed encoding of a random stimulus or some filtered and/or half-wave rectified version of it (such as temporal derivative encoding, band-pass filtering and on/off responses). The accuracy of the information transmitted about $s(t)$ was characterized in the time domain by the coding fraction, defined as $\gamma = 1 - \varepsilon/\sigma$, where ε is the root-mean-square error between the true and estimated stimulus, and σ is the standard deviation of $s(t)$ (ref. 1). The coding fraction takes the maximum value of 1 when the stimulus is perfectly estimated ($\varepsilon = 0$) and the minimum value of 0 if estimation from the spike train is at chance level ($\varepsilon = \sigma$) (refs 12, 13). We computed the coding fraction for P-receptor afferents and pyramidal cells; single P-receptor afferents were able to encode up to 75% of the stimulus time course, but pyramidal cells encoded less than 30%. Such a poor performance suggests that individual pyramidal cells do not convey detailed information on the time course of the stimulus to higher-order levels of the electrosensory system.

Pyramidal cells might transmit information about temporal features in the stimulus by performing a nonlinear classification task. This possibility can be tested by using neural network models. An artificial neural network can learn from the stimulus and response data to find the 'optimal' sensory input pattern eliciting a spike[14]. We used a more direct method derived from signal-detection theory, which assumes that the nonlinear classification task is implemented by means of a linear summation of incoming information plus a threshold computation[11,15]. To determine the optimal temporal feature $\mathbf{f}$ predicting the occurrence or non-occurrence of a spike in a pyramidal cell, we binned the data and studied the distributions of amplitude modulation waveforms preceding a bin containing a spike or no spike. We first determined the mean stimulus preceding a bin containing a spike ($\mathbf{m}_1$) and no spike ($\mathbf{m}_0$) (Fig. 1*b*) and then computed the covariance matrices $\mathbf{\Sigma}_1$ and $\mathbf{\Sigma}_0$ (Fig. 1*c*, *d*) characterizing second-order variations and correlations of these distributions around their means. The optimal $\mathbf{f}$ was determined as the direction in this temporal stimulus space of amplitude modulation waveforms for which the ratio of the mean squared distance between stimuli preceding a spike and no spike (computed from $\mathbf{m}_1$ and $\mathbf{m}_0$) and of their variances (computed from $\mathbf{\Sigma}_1$ and $\mathbf{\Sigma}_0$) was maximized (see equation (1) in 7Methods). This method is illustrated in a two-dimensional example (Fig. 2*a*, inset). For the I-type pyramidal cell depicted in Figs 1 and 2, the optimal sensory stimulus that predicted the occurrence of a spike, $\mathbf{f}$, was a downstroke in the

electric-field amplitude, preceded at around 100 ms by a small upstroke (Fig. 2*a*). For E-type pyramidal cells, the shape of the optimal feature was reversed. The time course of **f** (Fig. 2*a*) differs from the time course of the mean stimulus preceding a spike, $\mathbf{m}_1$ (Fig. 1*b*), because the former takes into account the mean stimulus preceding a bin containing no spike, $\mathbf{m}_0$, as well as second-order variations, Σ_1 and Σ_0. In general **f** did not differ significantly from zero for time values of 300 ms or more before the spike occurrence (Fig. 2*a*).

A large fraction ($56 \pm 21\%$, $n = 30$ cells) of the spikes generated by pyramidal cells in response to random amplitude modulations occurred in short bursts (mean number of spikes per burst, 2.9 ± 1.3; Fig. 1*a*, inset). To examine whether the occurrence of burst-like spike patterns signalled the presence of the temporal

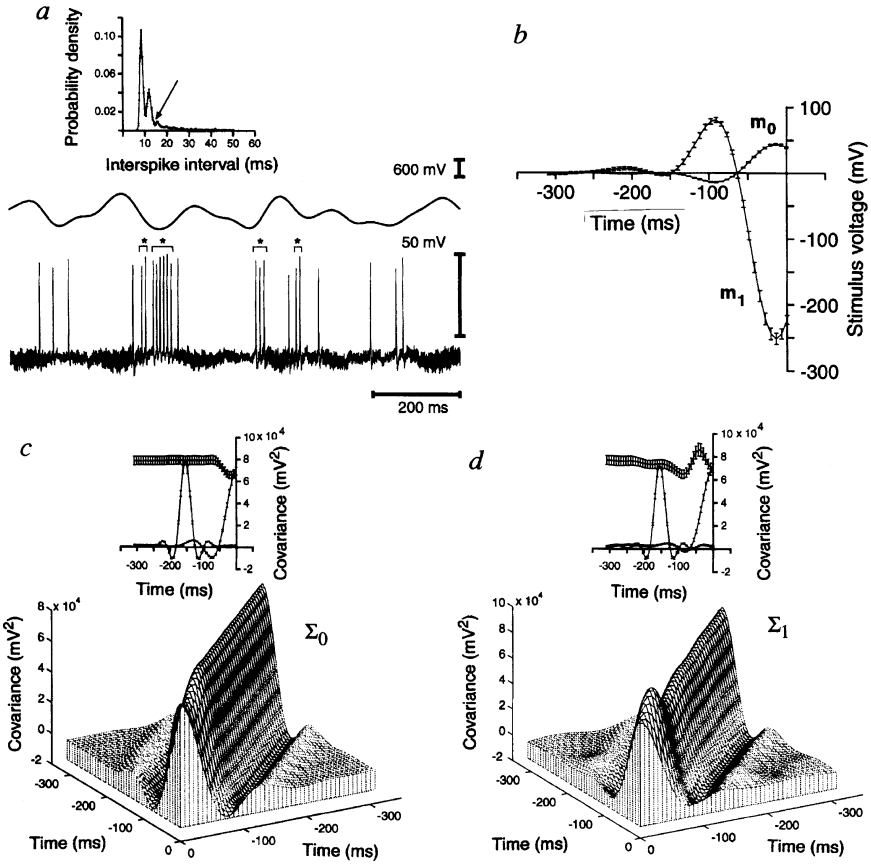

FIG. 1 Response of an I-type pyramidal cell in the lateral ELL segment to random amplitude modulations. *a*, Stimulus s(*t*) (centre). Standard deviation, 0.29 V (29% modulation of the mean amplitude at the pectoral fin, 1.25 mV cm^{-1}; ±1 V represents doubling and reduction to zero of the mean amplitude). Cut-off frequency, 12 Hz. Bottom, intracellular voltage. Asterisks denote burst spikes. The high-frequency noise is a stimulus artefact caused by the carrier of s(*t*) (425 Hz). Inset, interspike interval distribution (bin size, 0.5 ms). The peaks are used to define bursts. Arrow, maximum interspike interval separating spikes assigned to the same burst (14 ms). *b*, Estimated stimulus (mean ± s.d. over 10 repetitions) preceding a bin ($t = 0$) containing no spike ($\mathbf{m}_0$) or one spike ($\mathbf{m}_1$, stimulus reverse correlation). The peak time of $\mathbf{m}_1$ (14 ms) is consistent with earlier latency estimates[30]. *c*, *d*, Covariances of the no-spike (Σ_0) and spike distributions (Σ_1). Insets, mean value of the covariance estimates ±s.d. along the main diagonals and the $t = 0$ axis.

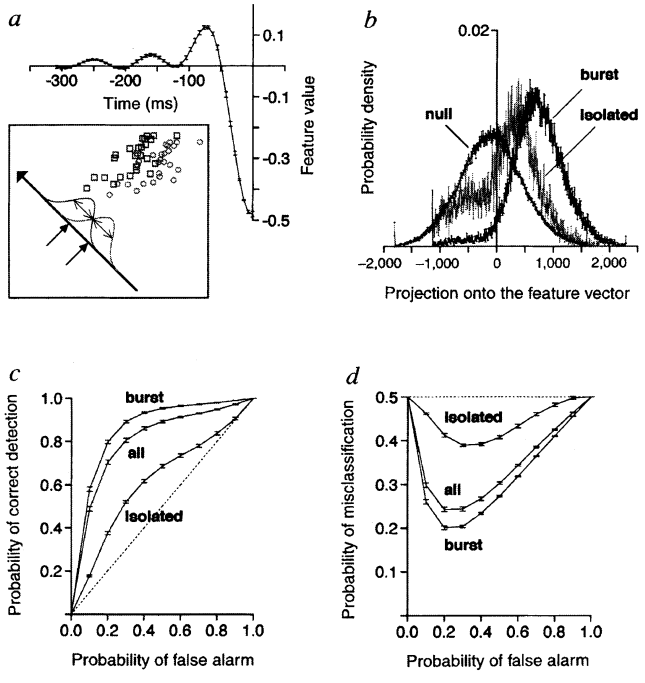

FIG. 2 Quantification of discrimination performance (cell used in Fig. 1). *a*, Optimal feature (normalized amplitude; see equation (1)). Inset, two two-dimensional gaussian distributions (circles and squares) are shown. The large arrow is the optimal feature maximizing the squared distance between the means (small single arrows) divided by their variances (double arrows); see equation (1). The distributions projected onto this feature would determine discrimination performance, as in *b*–*d*. *b*, Distribution of stimuli projected onto the optimal feature (bin width, 14). Stimuli preceding a bin containing no spike (null), an isolated spike, and a burst spike. *c*, ROC curves for the discrimination between the null distribution and the distributions of: isolated spikes; burst spikes; and all spikes (dashed line, chance level). They give the performance of an observer choosing a threshold along the horizontal axis of *b* and classifying a stimulus as eliciting a spike when the projection onto the feature is above threshold. Decreasing the threshold increases the probability of false alarm. *d*, Probability of misclassification plotted against probability of false alarm, given by (probability of false alarm +1 − probability of correct detection)/2 (see *c*).

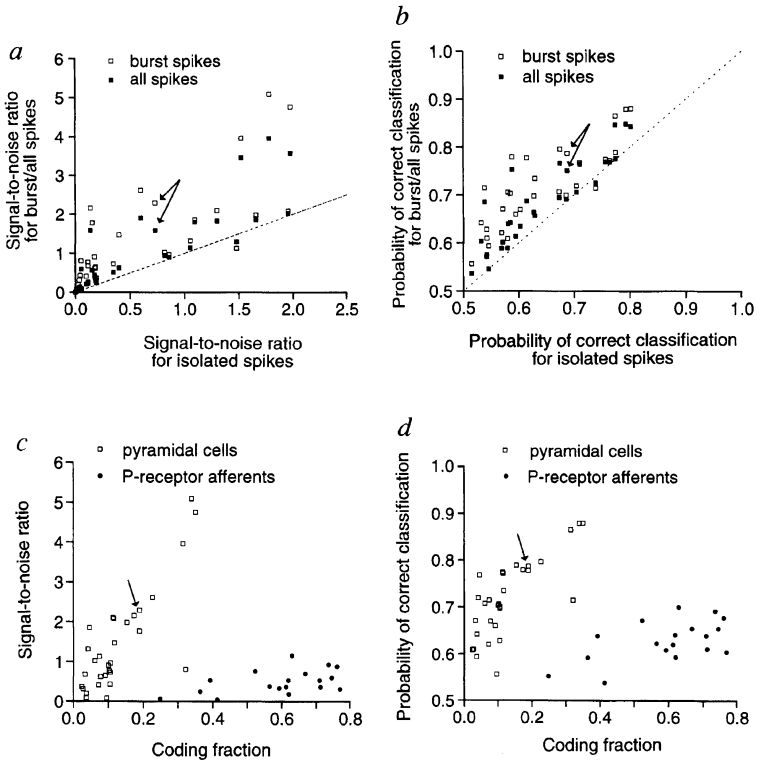

FIG. 3 Pyramidal cells ($n = 30$) extract temporal features from the stimulus time course encoded by P-receptor afferents ($n = 18$). *a*, Signal-to-noise ratios in the discrimination task (see equation (1)) for isolated spikes plotted against signal-to-noise ratio for burst spikes (open squares) and all spikes (filled squares). Dashed line, identical performance. Arrows, data points obtained from the cell used in Figs 1 and 2. *b*, Probability of correct classification for isolated spikes (1 – minimum probability of misclassification; see Fig. 2*d*) plotted against the probability of correct classification for burst spikes (open squares) and all spikes (filled squares). *c*, Signal-to-noise ratio as a function of coding fraction for pyramidal cells (open squares, burst spikes) and P-receptor afferents (filled circles). Note the weak and moderate correlation between these variables for P-receptor afferents and pyramidal cells (Pearson correlation coefficient, $\rho = 0.50$ and 0.80). For each pyramidal cell and P-receptor afferent the best performance in the discrimination task was selected. *d*, Probability of correct classification as a function of coding fraction (as in *c*; $\rho = 0.58$ and 0.76). Note the larger variability in the performance of pyramidal cells.

feature vector more reliably than isolated spikes, we separated the stimuli preceding a spike into two groups, depending on whether the spike was part of a burst or not, before computing their projection onto the feature vector (Fig. 2*b*). The distribution of stimuli associated with burst spikes had a significantly smaller overlap with the distribution of stimuli preceding no-spike containing bins (the null distribution in Fig. 2*b*) than the distribution of stimuli associated with isolated spikes. This was confirmed by comparing the receiver-operating characteristics curves describing the probability that an ideal observer will correctly identify a stimulus as eliciting a spike (probability of correct detection) for a fixed probability of incorrectly identifying a stimulus as eliciting a spike (probability of false alarm). For any false alarm rate, spikes from bursts were a better indicator for the presence of the optimal sensory stimulus than isolated spikes or all spikes taken together (Fig. 2*c*). This was also true when considering the probability of misclassification of a stimulus, given by averaging the probability of incorrectly identifying a stimulus as eliciting a spike (probability of false alarm) and the probability of incorrectly identifying a stimulus as eliciting no spike (one minus the probability of correct detection; Fig. 2*d*). In this particular example, the performance of all spikes taken together was close to the performance of spikes occurring in bursts, reflecting the fact that most spikes (77%) did occur in bursts. Similar results were found for all 30 pyramidal cells analysed and are summarized in Fig. 3*a*, *b*.

How accurately do processes at the input stage to the ELL (P-receptor afferents) convey explicit information about the presence or absence of temporal features? After repeating the same analysis on spikes of P-receptor afferents, we found that our sample population of P-receptor afferents ($n = 18$) was significantly outperformed in the discrimination task. The signal-to-noise ratio achieved by pyramidal cells in the discrimination task reached maximal values of 4.0 for all spikes combined, and up to 5.0 when only spikes belonging to bursts were considered (Fig. 3*a*, *c*). Accordingly, by integrating their inputs over the previous 300 ms and generating a spike, pyramidal cells could indicate the presence of the optimal feature with 85% accuracy, and up to 88% accuracy when only spikes belonging to bursts are considered (the chance level is 50%; Fig. 3*b*, *d*). But, for P-receptor afferents, the maximal signal-to-noise ratio in the discrimination task was only 1.2 and the discrimination accuracy 70% (Fig. 3*c*, *d*). The difference between the discrimination ability of all pyramidal cell spikes and of P-receptor afferent spikes was statistically significant (Wilcoxon rank-sum test, $\alpha \leq 0.025$), and the difference between pyramidal cell spikes belonging to bursts and P-receptor afferent spikes was highly significant (Fig. 3*d*, vertical axis; $\alpha \leq 0.0005$). In contrast, the fraction of the stimulus time course encoded by P-receptor afferents was always considerably higher than that encoded by pyramidal cells (Fig. 3*c*, *d*, horizontal axis). Thus the temporal features are extracted by the ELL circuitry from the detailed time-course information conveyed in the spike trains of P-receptor afferents.

We assumed that feature extraction resulted from a linear summation of incoming temporal information followed by a threshold computation. This computation could be performed at or near the soma of pyramidal cells using the threshold of the spike-generation mechanism. Such a simple model requires information on the detailed time course of the stimulus to be present in the somatic subthreshold membrane potential. To test this, we estimated the stimulus directly from the intracellular subthreshold membrane potential, obtained by removing the spikes from the membrane voltage trace. We then compared the coding fraction with that obtained from pyramidal cell spike events. The fraction of the stimulus encoded in the intracellular membrane potential was not significantly higher than that encoded in spikes (mean increase, $1.7 \pm 1.8\%$; $n = 20$ cells). It is therefore unlikely that temporal feature extraction was computed by means of a simple thresholding of the membrane voltage. In an *in vitro* preparation of the ELL from a closely related species, it has been demonstrated that retrograde propagation of somatic action potentials in conjunction with tetrodotoxin-sensitive conductances localized in the dendrites were responsible for short spike bursts similar to those observed here *in vivo*[16]. This observations, combined with our intracellular recordings, strongly suggests that feature extraction results from dendritic processing. Inhibitory control of dendritic pyramidal cell excitability[4,17] is likely to play an important role in this computation.

ELL pyramidal cells of weakly electric fish exemplify how active dendritic processing can solve a specific temporal pattern-recognition task[18]. The short bursts of spikes emitted in response to up-

and downstrokes of electric-field amplitude modulations represent code symbols[19] that can be expected to be robust against subsequent noise sources, such as those introduced by unreliability in synaptic transmission[20]. This robustness, which might explain the widespread occurrence of burst spike sequences in various sensory systems, is at the expense of temporal resolution. However, the resolution that can be inferred from the average burst duration (18 ± 9 ms first-to-last spikes in 30 cells) is sufficient for the detection of distortions of the electric field during electrolocation[4] and for the initiation of the jamming avoidance response[10]. In contrast, a substantially higher temporal resolution is achieved in the separate channel formed by T-type electroreceptor afferents and higher-order neurons distinct from those processing amplitude modulations[21]. The statistical analysis used here, complementary to the successful neuroethological approach[10], indicates that the electrosensory system in weakly electric fish may help us to understand better the links between biophysics and specific neural computations, such as temporal pattern recognition. □

Methods

Electrophysiology and stimuli. Extracellular recordings from receptor afferents and intracellular recordings from pyramidal cells were performed using standard electrophysiological techniques[1,22]. Intracellular recording electrodes were filled with neurotracer (neurobiotin; Vector) for intracellular labelling. This allowed to verify the cell type and its location within the ELL. Where no intracellular cell labelling could be performed, the recording site was verified by setting electrolytic lesions at the conclusion of the experiment using a high-frequency current source[23]. Standard histological methods were used and sections were analysed using light microscopy following the common nomenclature[24]. Electrode placements in the central region of the pyramidal cell layer of the ELL are expected to record activity of superficial and intermediate pyramidal cells[25]. Deep pyramidal cells were not included in our sample. A detailed description of the random stimuli used is given in ref. 1 (see equation (2)).

Data analysis. Data from each E- and I-type pyramidal cell from two different ELL segments (centromedial and lateral[26]) and from each P-receptor afferent were analysed to assess their ability to convey detailed information about the stimulus time course or the presence of temporal features in the stimulus waveform. Methods of stimulus estimation are described in refs 1, 12. For stimulus estimation from the subthreshold membrane potential, spikes were removed by two methods with similar results: median filtering of the membrane voltage trace; and threshold detection of spikes and linear interpolation of the voltage between the end points of a spike. To assess the ability to convey feature information, spike trains and stimuli of a duration of 135 s were binned using three bin sizes between $\Delta t_{min} = 0.5$ ms (the sampling rate) and Δt_{max} = maximal bin size, resulting in no more than one spike per bin. Of those, the size yielding best performance was retained[27] (in Figs 1 and 2, $\Delta t = 7$ ms). Maximum-likelihood estimators of the mean vectors (respectively of the covariances; ref. 15, section 3.2) had at most 100 (respectively 100×100) time components. The optimal feature $\mathbf{f}$ was obtained by maximizing the signal-to-noise ratio (SNR) (Fisher's linear discriminant function; see ref. 15, section 6.5; ref. 11, section IIIB) defined by,

$$\mathrm{SNR}(\mathbf{f}) = \frac{[\mathbf{f}\cdot(\mathbf{m_1} - \mathbf{m_0})]^2}{\mathbf{f}\cdot\frac{1}{2}(\Sigma_0 + \Sigma_1)\mathbf{f}} \quad (1)$$

The vector $\mathbf{f}$ that maximizes SNR($\mathbf{f}$) satisfies $(\mathbf{m_1} - \mathbf{m_0}) = 1/2(\Sigma_0 + \Sigma_1)\mathbf{f}$. This equation was solved numerically by diagonalizing $\Sigma_0 + \Sigma_1$ using MATLAB subroutines (that is, by performing a principal component analysis) and retaining the first n largest eigenvalues accounting for 99% of the variance (ref. 28, sections 6.1 and 8.1). The receiver-operating characteristics and the minimum probability of error were computed using the resubstitution method[29]. Typical sample sizes: null distribution, $N > 10,000$; isolated spikes, $N > 500$; burst spikes, $N > 2,000$.

Received 18 June; accepted 11 October 1996.

1. Wessel, R., Koch, C. & Gabbiani, F. *J. Neurophysiol.* **75,** 2280–2293 (1996).
2. Bialek, W., de Ruyter van Steveninck, R. & Warland, D. *Science* **252,** 1854–1857 (1991).
3. Zakon, H. in *Electroreception* (eds Bullock, T. H. & Heiligenberg, W.) 103–156 (Wiley, New York, 1986).
4. Bastian, J. in *Electroreception* (eds Bullock, T. H. & Heiligenberg, W.) 577–611 (Wiley, New York, 1986).
5. Hopkins, C. *Annu. Rev. Neurosci.* **11,** 497–535 (1988).
6. Maler, L., Sas, E. & Rogers, J. *J. Comp. Neurol.* **195,** 87–139 (1981).
7. Hopkins, C. *J. Comp. Physiol. A* **111,** 171–207 (1976).
8. Bastian, J. & Heilgenberg, W. *J. Comp. Physiol. A* **136,** 135–152 (1980).
9. Turner, R., Plant, J. & Maler, L. *J. Neurophysiol.* **76,** 2364–2382 (1996).
10. Heiligenberg, W. *Neural Nets in Electric Fish* (MIT Press, Cambridge, MA, 1991).
11. Poor, H. *An Introduction to Signal Detection and Estimation* (Springer, New York, 1994).
12. Gabbiani, F. & Koch, C. *Neural Computat.* **8,** 44–66 (1996).
13. Gabbiani, F. *Network: Comp. Neural Syst.* **7,** 61–85 (1996).
14. Lehky, S., Sejnowski, T. & Desimone, R. *J. Neurosci.* **12,** 3568–3581 (1992).
15. Anderson, T. W. *An Introduction to Multivariate Statistical Analysis* (Wiley, New York, 1984).
16. Turner, R. W., Maler, L., Deerinck, T., Levinson, S. R. & Ellisman, M. H. *J. Neurosci.* **14,** 6453–6471 (1994).
17. Maler, L. & Mugnaini, E. *J. Comp. Neurol.* **345,** 224–252 (1994).
18. Yuste, R. & Tank, W. *Neuron* **16,** 701–716 (1996).
19. Bair, W., Koch, C., Newsome, W. & Britten, K. *J. Neurosci.* **14,** 2870–2892 (1994).
20. Allen, C. & Stevens, C. *Proc. Natl Acad. Sci. USA* **91,** 10380–10383 (1994).
21. Kawasaki, M., Rose, G. & Heiligenberg, W. *Nature* **336,** 173–176 (1988).
22. Metzner, W. & Heiligenberg, W. *J. Comp. Physiol. A* **169,** 135–150 (1991).
23. Metzner, W. *J. Neurosci.* **13,** 1862–1878 (1993).
24. Maler, L, Sas, E., Johnston, S. & Ellis, W. *J. Chem. Neuroanat.* **4,** 1–38 (1991).
25. Bastian, J. & Courtright, J. *J. Comp. Physiol. A* **168,** 393–397 (1991).
26. Carr, C., Maler, L. & Sas, E. *J. Comp. Neurol.* **211,** 139–153 (1982).
27. Krueger, J. & Becker, J. *Trends Neurosci.* **14,** 282–286 (1991).
28. Jolliffe, I. *Principal Component Analysis* (Springer, New York, 1986).
29. Raudys, S. & Jain, A. *IEEE Trans. Patt. Anal. Mach. Intell.* **13,** 252–264 (1991).
30. Shumway, C. *J. Neurosci.* **9,** 4388–4399 (1989).

ACKNOWLEDGEMENTS. We thank J. Juranek for computer assistance, and M. Konishi, W. Kristan and G. Laurent for comments. This work was supported by grants from NSF, NIMH, UCR, the Center for Neuromorphic Systems Engineering as a part of NSF's Engineering Research Center program and the Sloan Center for Theoretical Neuroscience.

CORRESPONDENCE and requests for materials should be addressed to F.G. (e-mail: gabbiani@klab.caltech.edu).

Mutations in the kinase Rsk-2 associated with Coffin–Lowry syndrome

Elisabeth Trivier, Dario De Cesare, Sylvie Jacquot, Solange Pannetier, Elaine Zackai*, Ian Young†, Jean-Louis Mandel, Paolo Sassone-Corsi & André Hanauer

Institut de Génétique et de Biologie Moléculaire et Cellulaire, CNRS, INSERM, ULP, B.P. 163, 67404 Illkirch, France
* Clinical Genetic Center, The Children's Hospital of Philadelphia, 34th Street and Civic Center Boulevard, Philadelphia, Pennsylvania 19104, USA
† Centre for Medical Genetics, City Hospital, Nottingham NG5 1PB, UK

The Coffin–Lowry syndrome (CLS), an X-linked disorder, is characterized by severe psychomotor retardation, facial and digital dysmorphisms, and progressive skeletal deformations[1]. Genetic linkage analysis mapped the CLS locus to an interval of 2–3 megabases at Xp22.2. The gene coding for Rsk-2, a member of the growth-factor-regulated protein kinases, maps within the candidate interval, and was tested as a candidate gene for CLS. Initial screening for mutations in the gene for Rsk-2 in 76 unrelated CLS patients revealed one intragenic deletion, a nonsense, two splice site, and two missense mutations. The two missenses affect sites critical for the function of Rsk-2. The mutated Rsk-2 proteins were found to be inactive in a S6 kinase assay. These findings provide direct evidence that abnormalities in the MAPK/RSK signalling pathway cause Coffin–Lowry syndrome.

Genetic mapping studies place the CLS locus in Xp22.2, within an interval of approximately 3 cM, between DXS365 and DXS7161 (refs 2–4). During a search for expressed genes, the sequence of a subclone derived from a yeast artificial chromosome insert (YAC ywxd2527), included in a contig encompassing the CLS interval (E.T. *et al.*, manuscript in preparation), showed 100% homology with a complementary DNA coding for Rsk-2 (ref. 5); this localization has been confirmed independently[6].

Rsk-2 is a member of a family of growth-factor-regulated serine–threonine kinases, known as $p90^{rsk}$ or RSK (for ribosomal S6 kinase). Homologues of RSK exist in several species[5,7–11]. In humans the RSK family comprises three closely related members: Rsk-1, Rsk-2 and Rsk-3 (refs 10, 11). The cDNA that encodes *Rsk-2* has an open reading frame of 2,220 bases, encoding a protein of 740 amino acids[5]. A highly conserved feature of all members of the RSK family is the presence of two non-identical, kinase catalytic domains[12]. RSKs